



Fabrication of high-performance nanofiber-based FO membranes

Raed M. El Khaldi^{a,e}, Mehmet E. Pasaoglu^{a,b}, Serkan Guclu^{a,b}, Yusuf Z. Menciloglu^c,
Reyhan Ozdogan^d, Mithat Celebi^d, Mehmet A. Kaya^d, Ismail Koyuncu^{a,b,*}

^aCivil Engineering Faculty, Environmental Engineering Department, Istanbul Technical University, 34469 Maslak, Istanbul, Turkey, Tel. +90 285 3417; emails: koyuncu@itu.edu.tr (I. Koyuncu), raedmkhaldi@iugaza.edu.ps (R.M. El Khaldi), mpasaoglu@itu.edu.tr (M.E. Pasaoglu), gucluse@itu.edu.tr (S. Guclu)

^bNational Research Center on Membrane Technologies (MEM-TEK), Advanced Technology Center, 34469 Maslak, Istanbul, Turkey, Tel. +90 285 3473

^cFaculty of Engineering and National Sciences, Sabanci University, 34956 Tuzla, Istanbul, Tel. +90 483 9000; email: yusufm@sabanciuniv.edu

^dEngineering Faculty, Polymer Engineering Department, Yalova University, 77200 Yalova, Turkey, Tel. +90 226 8155400; emails: reyhanozdogan16@gmail.com (R. Ozdogan), mithat.celebi@yalova.edu.tr (M. Celebi), marifkaya@yalova.edu.tr (M.A. Kaya)

^eEnvironmental and Earth Sciences Department, Islamic University of Gaza, 108 Gaza Strip, Palestine, Tel. +90 5511676829

Received 24 May 2018; Accepted 27 December 2018

ABSTRACT

Being partially commercialized and has specific application areas, where the reverse osmosis technology cannot serve, forward osmosis (FO) technology is continually receiving extensive research to promote its performance. In this study, high-performance FO nanofiber-based substrate membrane was fabricated for potential application of saline water desalination. Sulfonated polysulfone (sPSU) with definite sulfonation level was used to fabricate support layer. Tubular beadless fiber network owning scaffold-like structure with a fiber diameter of 247 nm was formed. Polysulfone was sulfonated by heterogeneous method using chlorosulfonic acid as a sulfonation agent. The substrate and FO membranes were characterized mainly by means of scanning electron microscopy (SEM), water permeation flux, porometry, contact angle, Fourier transform infrared (FTIR), as well as other tests, while the characterization of thin-film composite separation layer was restricted to SEM and FTIR. The characterization illustrates that the sPSU support layer is highly porous with a narrow pore size distribution. FO performance evaluation of two commercial and newly developed membranes was probed using FO and pressure-retarded osmosis (PRO) modes with cocurrent and counter-current flow scheme. The active layer presents excellent intrinsic properties with A/B of 17.31 and a high salt separation ratio of 99.54%. The newly developed membrane can achieve a high FO and PRO water flux of 65.7 and 313 L m⁻² h⁻¹, respectively, using a 1 M NaCl draw solution and deionized water feed solution. The corresponding salt flux is only 2.5 and 5.3 g m⁻² h⁻¹. The reverse flux selectivity represented by the ratio of water flux to reverse salt flux (J_w/J_s) was kept as high as 26.3 and 58.8 L g⁻¹ for FO and PRO modes. To the best of our knowledge, the performance of the current work-developed membrane is superior to all FO membranes previously reported in the literature.

Keywords: Forward osmosis membrane; Pressure-retarded osmosis; Electrospinning; Nanofiber; Interfacial polymerization; Polyamide; Sulfonated polysulfone

* Corresponding author.

1. Introduction

Freshwater reserves are rapidly shrinking all over the world. Sea water desalination is the most powerful alternative that may constitute an ideal solution to the water scarcity. Although there are several processes to desalinate sea water, such as reverse osmosis (RO) [1], forward osmosis (FO) [2], nanofiltration [3], ion exchange [4], electrodialysis [5], thermal desalination [6], and multistage flash distillation [7], there is still an urgent need to develop the existing approaches or introduce a new cost-effective one. Any candidate desalination method should outperform their old counterparts through securing high production efficiency and low energy consumption.

FO is an emerging membrane technology platform that may play complementary role to RO and/or offers a low-cost alternative in specific applications where there is no need of large external hydraulic pressure. FO process has two modes, (1) FO mode, where active layer facing feed solution (AL-FS), and (2) pressure-retarded osmosis (PRO) mode, where active layer facing draw solution (AL-DS), that required no or low pressure energy [8].

Two materials make up the bulk of commercial osmosis-driven membranes, cellulose acetate (CSA) and an aromatic polyamide. The first commercial desalination membrane was a symmetric CSA that was fabricated by forming a simultaneous porous support layer and a dense skin layer during the solvent and the coagulant medium exchange [9]. CSA-based membrane showed low water permeation due to its high concentration polarization. Being a more easily tailoring and high efficient performance in terms of water flux and salt separation, thin-film composite (TFC) membrane was discovered by John Cadotte. The TFC membranes have several advantages over CSA membranes as they have a better water flux, a higher working temperatures, and a wider tolerance toward pH [10].

The basic construction of the TFC membranes comprises three sequential fundamental layers: (1) a backing nonwoven material for strength, (2) a porous polymer-based support formed on top of the backing material, and (3) top ultrathin selective barrier layer [11].

Phase-inverted porous middle layer can be overlaid by ultrathin separation layer via interfacial polymerization or coating techniques such as photo grafting, dip coating, electron beam irradiations, and plasma-initiated polymerization [12].

Synthesis of polyamide-based TFC membrane by interfacial polymerization successfully fabricated through the reaction between two monomers, a polyfunctional amine and a polyfunctional acid chloride, dissolved in water and hydrocarbon solvent, respectively [13].

Redesign of FO membrane either in terms of the dense layer or in the substrate ought to be enhanced based on productivity (a high water flux) and quality (a low reverse salt flux (RSF)). A low water flux results mainly from internal concentration polarization (ICP). This phenomenon took place essentially in the substrate layer and considered one of the most limiting factors for the FO process performance and application. Unlike external concentration polarization, ICP cannot be treated by controlling the cross-flow velocity (CFV) and turbulence along the membrane surface [14]. Mitigation

of the ICP effect can be achieved through the modification of the substrates' structure and chemistry [15].

McCutcheon and Elimelech [16] studied the influence of membrane support layer hydrophobicity on water flux in osmotically driven membrane processes. Their results revealed that support layer hydrophilicity plays a crucial role in water flux across asymmetric semipermeable membranes.

Recent application of new emerging materials such as electrospun nanofiber membranes (ENMs) has been continually expanding in membrane industry. Owing to its large internal surface area to volume, low tortuosity, and high porosity, ENMs are a candidate to replace conventional membrane material in different membrane structures and processes. In addition, it could be introduced as a substitute or another alternative for the phase-inverted porous-supported TFC in various membrane process applications [17,18].

Hydrophilicity of the membrane polymer can differ with respect to membrane-forming process and resultant pore structure. For instance, while the contact angle of the PS substrate used as a mid layer in TFC membrane can range from 50° to 70° as it fabricated by phase inversion (sponge or finger-like pore structure), the same polymer can show a surface contact angle range from 110° to 140° when the membrane was fabricated by electrospinning technique (scaffold-like pore structure). In general, ultrathin separation film forming on the top of the phase-inversion support layer was easily accomplished in hydrophilic polymer, while it was not viable in case of hydrophobic material without further surface modification.

Subramanian and Seeram [18] concluded that fabrication of thin film nano composite membrane with high selectivity and water permeation required post-heat treatment of electrospun nanofiber and increase in its hydrophilicity, in addition to reduction of cross section and fiber thickness.

Sulfonated electrospun nanofiber composite membranes widely used for fuel cell applications suggest that they are able to achieve a high proton conductivity, low gas permeability into the fuel, and good chemical and thermal stabilities [19].

Recently, much effort has gone into the development of sulfonated material to be used in FO-TFC substrate due to their high hydrophilicity and potential production of low structure parameter (*S*-value) that could restrict the ICP effect and enhance water flux.

Chen et al. [20] found that increasing the amount of hydrophilic sulfonated polysulfone in the polymer blend of sPSU/PSU lead to increase water flux and decrease the salt separation. sPSU make swelling of the membrane in water, thereby yielding a higher water flux. They also observed that larger channels were formed resulting in a lower salt rejection.

Widjojo et al. [21] used sulfonated polyphenylsulfone with 11 wt.% sulfonation degree as a copolymer with polyethersulfone (PES) to fabricate sponge-like structure substrate of TFC-FO flat-sheet membrane. Their results showed that TFC-FO membranes with 50 wt.% (sPPSf) ran under PRO mode provided water flux of 33.0 L m⁻² h⁻¹ (LMH) against DI water and 15 LMH against the 3.5 wt.% NaCl-simulated solution using 2 M NaCl as the draw solution.

Recently, the same working team fabricated new membrane similar to the former one with some minor material modifications that achieved water flux of 54 LMH and 22 LMH under the same previous conditions and operating mode [22].

PSf blended with 50 wt.% sulfonated poly(etherketone) with 10 wt.% sulfonation degree was selected as the support layer material to synthesise (FO-TFC) membranes for desalination [23]. The results demonstrate that the membrane attains water flux of 50 LMH against deionized water (DW) and 22 LMH against 3.5 wt.% NaCl model solution when using 2 M NaCl as the draw solution in the AL-DS mode.

The current paper presents the results related to FO nanofiber-based substrate membrane fabricated totally from sPSU. Unprecedented high water flux and salt rejection make this membrane particularly suitable for sea water desalination operated by FO where low water flux and the propensity for fouling are the major concerns.

2. Experimental

2.1. Materials and methods

Polysulfone (PSf) from Solvay (France) and dimethylacetamide (DMAc) from Ak-kim (Turkey) were used for the preparation of the membrane substrate. For TFC layer fabrication, two solutions were prepared. *m*-Phenylenediamine (MPD) (Merck, USA), triethylamine (TEA) (Merck, USA), (+)-10-camphorsulfonic acid, 99% (Sigma-Aldrich, Germany), and sodium dodecyl sulfate (SDS) (Sigma-Aldrich, Germany) were used to prepare MPD aqueous solution, while (0.1 w/v) TMC organic solution was prepared by mixing

1,3,5-benzenetricarbonyl trichloride (Aldrich, Germany) with hexane-anhydrous, 95% (Sigma-Aldrich, Germany). For FO characterization tests, sodium chloride (NaCl) supplied by Merck (USA) was used for draw solution preparation.

A commercial polyester nonwoven fabric (PET, Ahlstrom, Helsinki, Finland) was used as a backing layer for the sPSU substrate. Commercial TFC FO membranes (Hydration Technology Innovations (HTI, USA) TFC-ES 130927) and asymmetric cellulose triacetate (HTI CTA, USA) FO membranes were acquired from Hydration Technology Innovations (Albany, OR) for comparison.

2.1.1. Sulfonation of PSf

PSf was sulfonated by a heterogeneous method with chlorosulfonic acid (Fig. 1). The commercial PSf was dispersed in concentrated sulfuric acid at room temperature and stirred vigorously. Chlorosulfonic acid was transferred into a dropper and then added dropwise to the resultant solution while stirring the solution at 800 rpm at 10°C. Thereafter, the mixture was gradually precipitated in DW, and the polymer was separated by filtration.

2.1.2. Preparation of sPSU membrane substrate and posttreatment

Dried at 70°C overnight in a vacuum oven, sPSU (30 wt.%) with a definite degree of sulfonation was dissolved in DMAc by stirring at 30°C for 48 h. Electrospinning setup (Fig. 2) was used to fabricate ENM substrate onto a PET

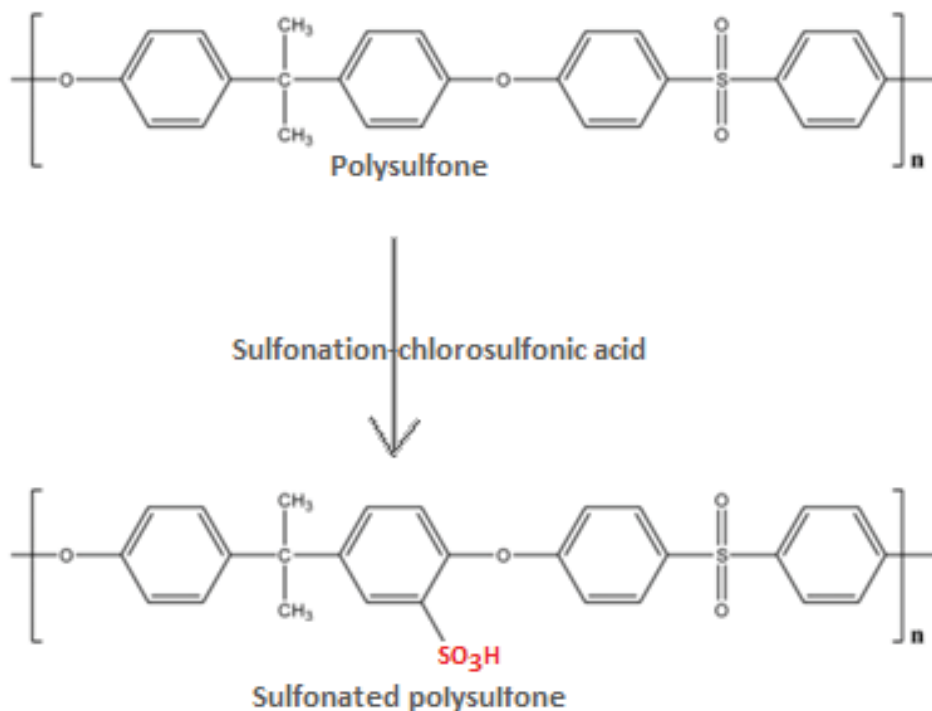


Fig. 1. Figure shows sulfonation process on polysulfone.

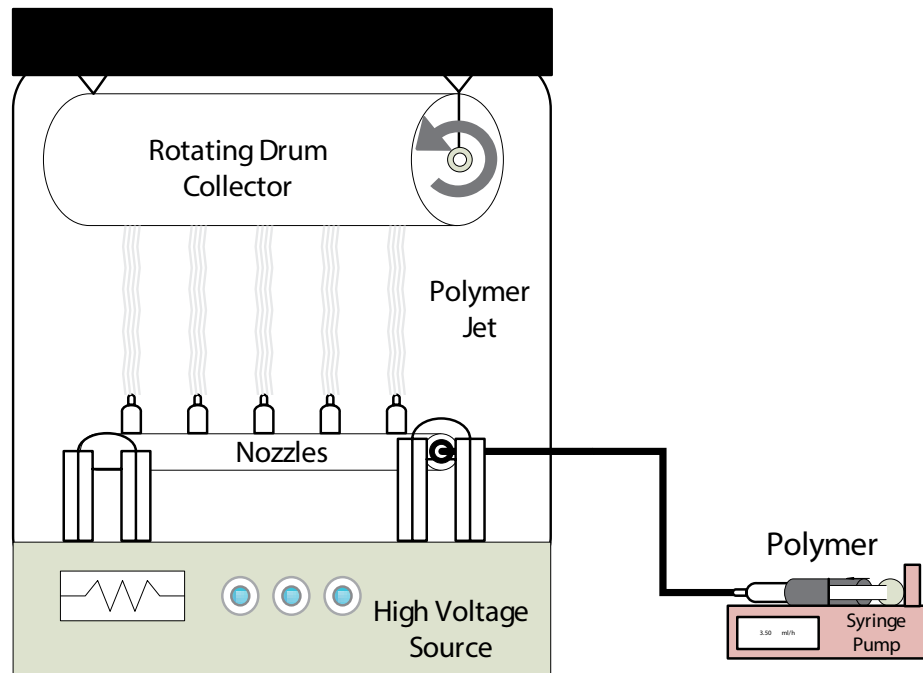


Fig. 2. Schematic of electrospinning setup used for sPSU substrate fabrication.

nonwoven support. The electrospinning conditions were as follows: spinning solution flow rate of 4 mL min^{-1} ; voltage 27 kV; tip-collector distance, 19 cm; and temperature, 25°C .

For better dimensional stability and structural integrity, the membrane was post-heat treated in the oven at 187°C for 3 h. Membrane perimeters were restrained to glass plate using binder clips to prevent membrane shrinking or warping due to stress relaxation (Fig. 3).

2.1.3. Fabrication of TFC membranes

Prior to the TFC layer synthesis, sPSU membrane substrate was kept in distilled water for 24 h for better wetting. Removal of air bubbles from distilled water that is used for the preparation of MPD solution was performed by driving nitrogen gas for 10 min before adding the rest of the

chemicals. After cleaning of TMC solution bottles, little amount of hexane was used to wash and remove any remaining distilled water and further TMC added into hexane during mixing for even distribution and homogeneity.

Formation of polyamide separation layer developed by the interfacial polymerization reaction between MPD and TMC on the top of electrospun substrate is shown in Fig. 4. First, the membrane substrate was soaked in a (2 w/v) % MPD aqueous solution for 5 min (100 mL of aqueous solution consists of 2 g MPD, 2.75 mL TEA, 0.1 g SDS, 2 g CSA, and 96 mL DW). Then, the excess water droplets on MPD-soaked supported membranes were rolled out with a rubber roller after placing the membrane on a filter paper.

Immediately, the membrane was fixed tightly to the rubber frame to bring only the top surface of the substrate membrane into contact with a (0.1w/v) % TMC/hexane

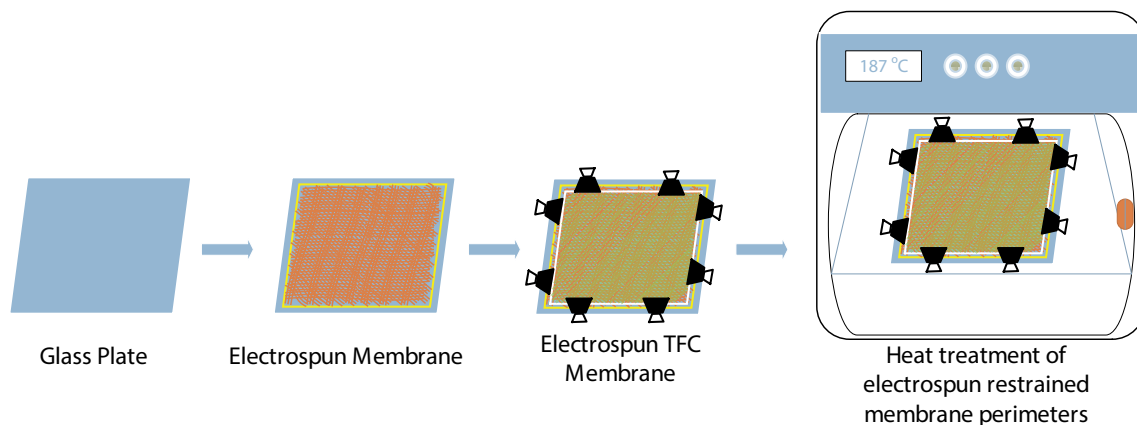


Fig. 3. Heat treatment of electrospun restrained membrane perimeters.

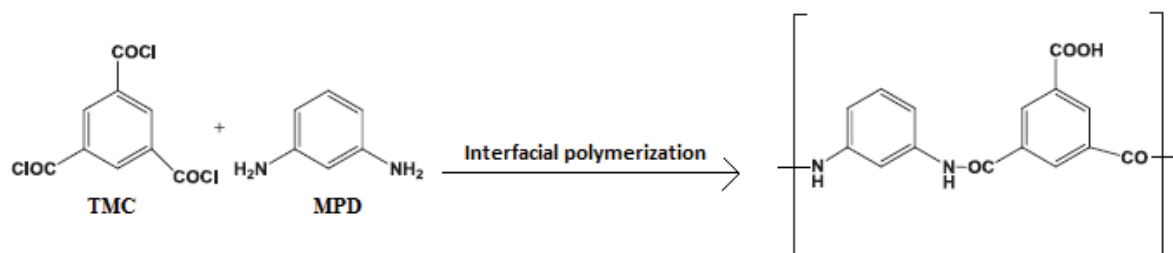


Fig. 4. Interfacial polymerization reaction scheme to form the polyamide separation layer.

solution for 2 min to avoid the penetration of the TMC/hexane solution for the nonwoven polyester. The composite membrane was then sequentially cured for 7.5 min into drying oven at 70°C.

The FO membranes were lastly stored in DW at room temperature for further characterization.

2.1.4. FO setup (operation conditions)

Water flux and reverse salt leakage were measured for commercial and laboratory-scale-fabricated electrospun-PSU-based TFC membranes using FO setup shown in Fig. 5. The membrane cell has rectangular flow channels (9 cm in length, 6.45 cm in width, and 0.3 cm in depth) with an effective membrane area of 0.0058 m² on both sides of the membrane. Two Viton O-rings were placed on outer perimeter of the cell to prevent leakage between FS and DS streams. Diamond-patterned spacers were put on both sides of the membrane to fill the flow channel and to simulate the mass diffusion across the membrane in spiral-wound FO elements [24]. The salt concentration changes in both the feed and draw solutions were measured by EC meter (Hach, HQ 40d multi), while weight changes in the feed compartment were recorded by digital balance (FX5000i, A&D Company Ltd., Japan). Feed and draw solutions flowed cocurrently and counter-currently in both FO mode and PRO mode using a peristaltic tubing pump (Cole Parmer, Masterflex L/S, Canada) at a constant circulation rate (600 rpm at feed side and 280 rpm at the draw side which meets 16.12 and 7.86 cm s⁻¹ as a CFV) and initial volume either for draw solution or feed solution (1.5 L in feed compartment and 0.5 L in draw compartment). With the progressing of the FO setup running, the initial concentration of draw solution (osmotic pressure) decreases as a consequence of water extraction from the feed solution side to draw solution side. All characterization tests were conducted at the room temperature using 1 M NaCl as a draw solution and distilled water as a feed solution.

2.1.5. Membrane performance parameters

Intrinsic properties of the TFC selective layer represented by water and salt permeability coefficients were determined. Measurement of A coefficient [Eq. (1)] was done in RO mode using a dead-end stirred-cell filtration system (sterlitech HP4750). The effective membrane area was 14.6 cm². Next to membrane compaction at 1 bar, pure water fluxes were measured at three different pressure

points (0.3, 0.6, and 0.9 bar). The membrane water permeability, A , was computed from the plot gradient of water flux (J_w) against applied pressure (P).

$$A = \frac{J_w}{\Delta P} \quad (1)$$

where J_w and ΔP represent the volumetric water flux and the applied transmembrane pressure, respectively.

The membrane solute permeability coefficient, B , was evaluated using the water flux and salt rejection percentage measurements following Eq. (2) [25].

$$B = J_w \times \left(\frac{1-R}{R} \right) \quad (2)$$

Where R is the salt rejection percentage.

The water permeate flux (J_w , L m⁻² h⁻¹, LMH), which is measured using aforementioned FO cross-flow setup (Fig. 5), was calculated from Eq. (3).

$$J_w = \frac{\Delta V}{(\Delta T \times A_m)} \quad (3)$$

where ΔV represents the permeation water extracted over a predetermined time Δt (h) and A_m is the effective membrane surface area.

The RSF (J_s , g m⁻² h⁻¹, abbreviated as gMH) was also calculated from Eq. (4).

$$J_s = \frac{[C_F (V_{F0} - J_w \times A_{Fm} \times \Delta T)]}{(A_m \times \Delta T)} \quad (4)$$

where C_F is the bulk feed solute concentration (C_{F0} is the initial NaCl concentration), V_{F0} is the initial volume of the feed solution, and the rest of the abbreviations were defined earlier.

Salt rejection rate (R , %) was calculated from Eq. (5), where m , L , and M are mole NaCl transferred to feed, water removed, and molarity of draw solution, respectively.

$$R = \left\{ 1 - \left[\frac{\left(\frac{m}{L} \right)}{\left(\frac{M}{M} \right)} \right] \right\} \quad (5)$$

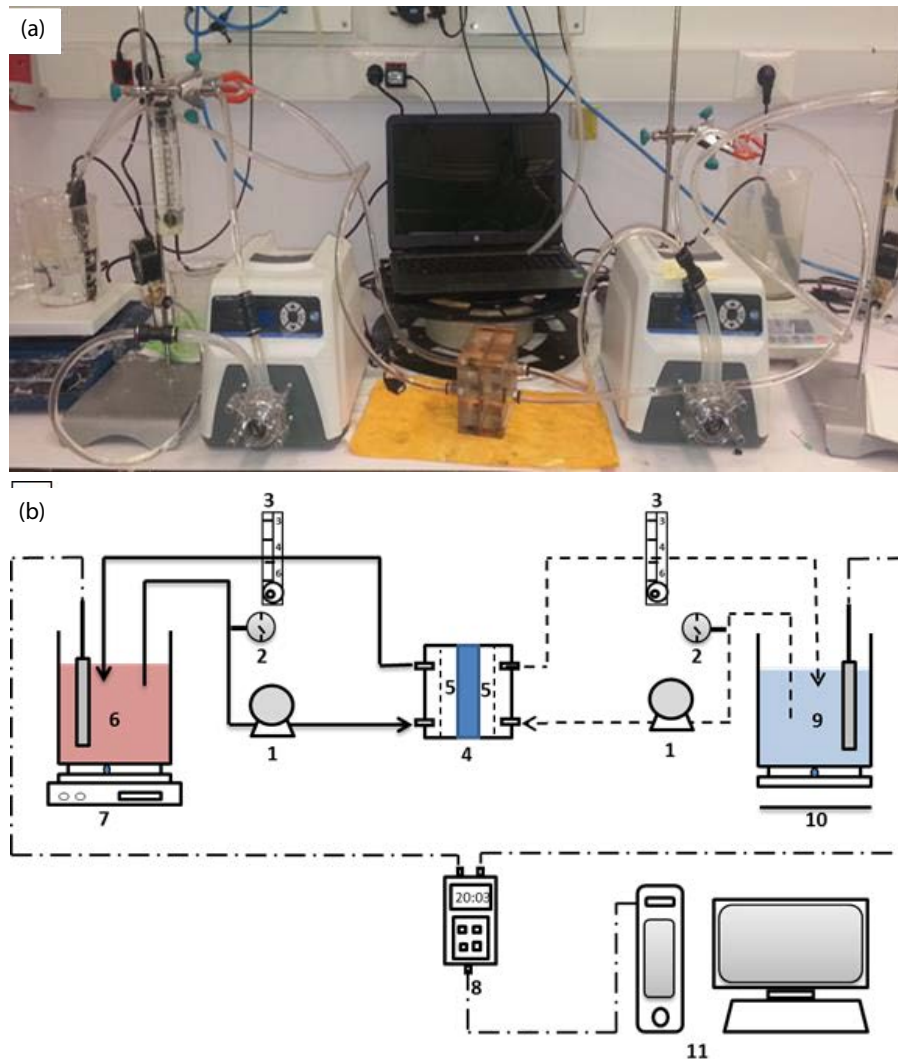


Fig. 5. (a) real photo of the laboratory-scale FO system and (b) schematic of the FO test unit: (1) circulating pump; (2) flow meter; (3) flow meter; (4) FO membrane; (5) flow chamber of FO test unit (membrane cell); (6) draw solution reservoir; (7) magnetic stirrer; (8) EC meter; (9) feed solution container; (10) weighing balance; and (11) computer.

3. Characterization of membranes

TFC and fiber morphology of produced membranes done with scanning electron microscope (SEM) images were observed with an FEI Quanta FEG 250 SEM after being coated with Au–Pd by using Quorum SC7620 ion sputtering.

Pure water flux was characterized in dead-end filtration cells (Sterlitech Corp., Kent, USA). Approximately 1,000 mL of ultrapure water was allowed to permeate through the membranes at 0.6 bar for compaction. For each membrane, water flux experiments were performed at 0.2, 0.4, and 0.6 bar. Using Microsoft Excel, flux versus pressure was plotted. From the slope of the graph, permeability results were obtained.

Pore size and distribution of the nanofibrous membranes have been studied using capillary flow porometry. Quantachrome's Porofil with a defined very low surface tension 16 dyne cm^{-1} (Quantachrome Ins., Florida, USA) was

used as the wetting agent for porometry measurements. Membranes were cut into $3 \text{ cm} \times 3 \text{ cm}$ squares for porometry measurement. The thickness of the prepared samples was measured electronically using the micrometer.

To examine the hydrophilicity of the membranes, water contact angle measurements were recorded using a tensiometer produced by Attension, KSV, Espoo, Finland, Instruments. A droplet of distilled water was formed on the tip of a stainless steel syringe needle and placed onto the membrane surface by free falling. From 3 different places on each membrane surface, 10 images were picked out and averaged to give mean contact angle. In order to further confirm the effect of substrate sulfonation, a non-sulfonated PSf nanofiber mate was electrospun under the same electrospinning operation conditions used in sPSU membrane and then contact angle measured for both of them.

Fourier transform infrared (FTIR) spectra were recorded for the dry support layer membrane to verify the

chemical structure of organic molecules and potential structural changes that occur as a result of the sulfonation process. FTIR spectra was measured in the absorbance mode ranging from 400 to 4,000 cm^{-1} at room temperature using PerkinElmer, (USA) Spectrum 100 FTIR Spectrometer.

Zeta potential analysis as an indicator of membrane fouling tendency and liquid phase adsorption processes were carried out using SurPASS from Anton Paar. It gives insights into the membrane surface chemistry and helps to understand and improve surface properties.

Calculation of membrane substrate porosity was done by utilizing the measurement of membrane weights in both dry and wet states according to Eq. (6).

$$\varepsilon = \frac{(m_1 - m_2)}{\frac{\rho_w}{(m_1 - m_2)} + \frac{m_2}{\rho_m}} \times 100\% \quad (6)$$

where m_1 and m_2 are the weights of wet and dry membranes and ρ_w and ρ_m the densities of water (1 g cm^{-3}) and the sPSU blend (0.94 g cm^{-3}), respectively.

4. Results and discussion

4.1. Effect of support layer type on FO membrane performance

4.1.1. Preliminary membrane fabrication and characterization trails to identify the right electrospinning dope solution recipe

The preparation of electrospinning dope revealed that sulfonation of PSf dropped the polymer solution viscosity and increased its electrical conductivity. The prepared dope solution showed a viscosity of 3,000 centipoise (Cp) with noticeable high electrical conductivity ($530 \mu\text{s cm}^{-1}$). With this dramatic changes of polymer properties, the sPSU was not able to be electrospun at the same polymer ratio of its original PSf polymer (up to 23%). To improve the electrospinnability of the sPSU solution and compensate for viscosity drop, two solution preparation methods were used. The first was enhancing viscosity via increasing polymer concentration ratio up to 30%, while the other method increased the polymer viscosity depending on adding small amount of high molecular weight polymer to the sPSU solution. Poly(ethylene oxide) (PEO) was used to enhance the second dope viscosity. In addition to these two sPSU solutions, 8% polyacrylonitrile (PAN) dope was prepared to be the third solution that would be tested to form a proper support membrane for synthesis of FO membrane.

The dope formulations (of the 3 substrates) are sPSU/DMAc with a weight ratio of 30/70, sPSU/PEO/DMAc with a weight ratio of 18/2/80, and PAN/DMF with a weight ratio of 8/92. They will be referred to as 30% sPSU, 20% sPSU/PEO, and 8% PAN, respectively.

In this stage, as an initial evaluation, fabricated membranes just only characterized against SEM and FO performance to check validity of dope viscosity enhancement and potential use of these membranes in the FO process. The membrane with best performance intended to undergo more extensive characterization in terms of substrate, TFC separation layer, and FO performance.

The TFC layers were developed with submersion substrate membranes for 10 min in MPD and 2 min reaction time with TMC following the same procedure and chemical preparation mentioned above. Fig. 6 displays the SEM micrographs of the support layer mates, surface TFC view, and TFC cross sections. The surface view of electrospun substrates for the three membranes showed scaffold structure with beadless tubular smooth surface. The top TFC layer view also revealed formation of defect-free polyamide layer. Thickness variance can be observed in the cross-sectional structure of the TFC layer. The mean TFC membrane cross-sectional values were 574, 2,200, and 2,200 nm in 8% PAN, 20% sPSU/PEO, and 30% sPSU, respectively. Comparing commercial TFC-RO membrane which has 0.2–0.25 μm polyamide layer, an 40–50 μm porous phase-inverted layer, and an 100- to 150- μm -thick nonwoven polyester fabric backing layer, the TFC layer thickness in the fabricated sPSU accounted for more than 10-fold [26].

FO membrane performance explored only under the cocurrent FO mode using DI water and 1 M NaCl as feed and draw solutions, respectively. As can be observed from the Table 1, 30% sPSU membrane obtained very high pure water flux compared with the other two membranes, while all the membranes gave a good rejection and RSF.

Fig. 7(a) shows that within approximately 3 h continuous operation time the J_s values were constant and small, which reflect minimum effect of ICP that allow long operation period before stopping the system for cleaning in these membranes. As well, high harmony between J_w and draw EC curves, particularly in 30% sPSU, reflected that osmotic flux linearity was related to draw solution concentration. The 20% sPSU/PEO and 8% PAN membranes revealed no big difference of the pure water permeation flux between the start and the end of the FO experiments. This may be due to low water flux. The variance of pure water permeation flux was obvious in the 30% sPSU as it has begun with initial flux of 93 LMH and end flux of 34 LMH going in agreement with decline of DS concentration. The pure water flux values in Table 1 are taken as an average for the records obtained during experimental operation. All the three membranes obtained high rejection rates, which emphasizes the SEM micrographs that defect-free TFC layer is properly formed. Attempt for new membrane fabrication will be carried out using 30% sPSU membrane for full characterization.

4.1.2. Characterization of best support layer type

Being achieved the best FO performance, the same sPSU dope ratio (30%) was used to fabricate a new TFC substrate, applying the same TFC layer synthesis conditions. The substrate and separation layers of the new FO membrane underwent more extensive characterization.

Morphology and fiber diameter distribution of sPSU membrane substrate, electrospun in this study, is displayed in Fig. 8. Tubular beadless fiber network owning a scaffold-like structure with fiber diameter of 247 nm was formed. The thickness of fiber diameter relies mainly on the spinning solution viscosity and conductivity, in addition to electrospinning operating conditions. The increase of solution conductivity can give a good chance to spin a thinner

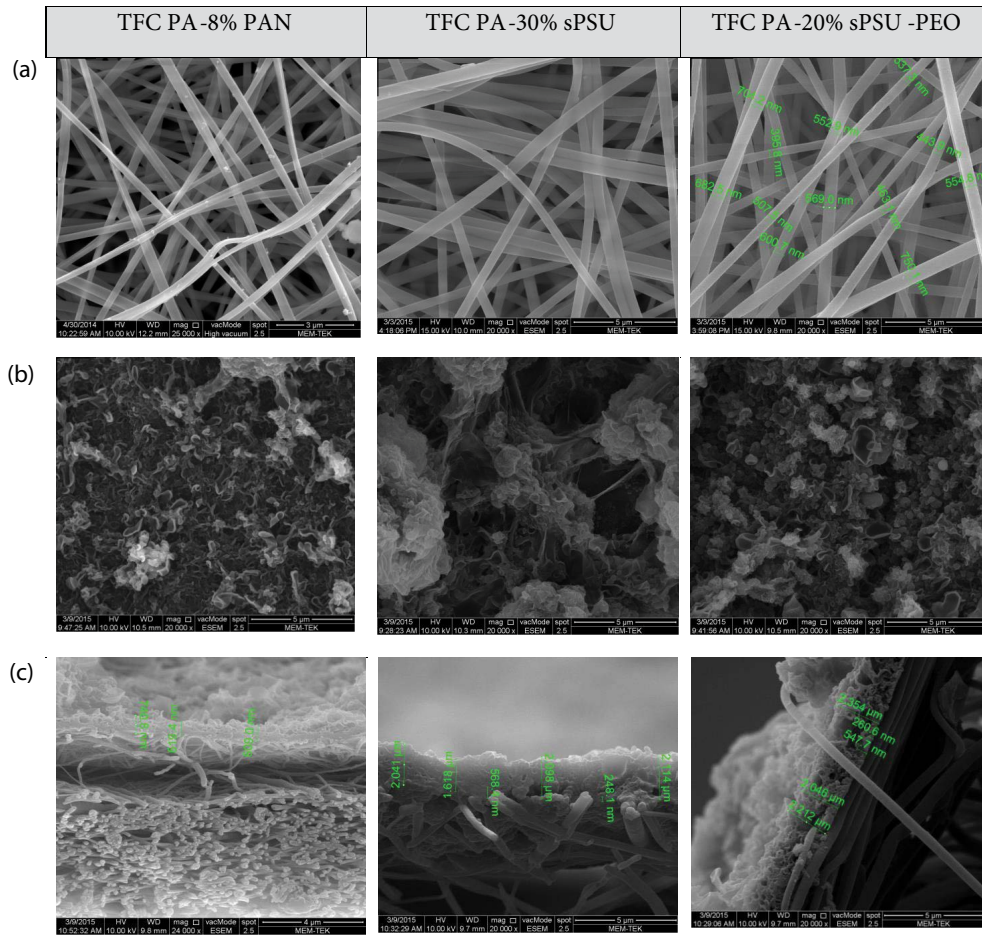


Fig. 6. SEM images of (a) top view of electrospun substrate, (b) top view of TFC separation layer, and (c) cross-sectional view of TFC separation layer.

Table 1
Performance of flat-sheet FO membrane in the current work under cocurrent flow mode

	TFC PA-8% PAN	TFC PA-30% sPSU	TFC PA-20% sPSU-PEO
Flux (LMH)	5.77	52.02	4.27
Rejection %	99.783	99.94	99.84
RSF (gMH)	1.03	0.44	0.55
J_s/J_w	0.178	0.008	0.129

fiber diameter. Shabani et al. [27] reported that with a low sulfonation degree (about 15 mole, %), PES solution conductivity increased from 3.32 to 152.5 $\mu\text{s cm}^{-1}$. Decrease in fiber diameter can be considered a positive sign in such membranes as it may decrease the average pore size between nanofibers that in one hand can enhance the backing functionality of the support layer and on the other hand facilitates bridging of interfacial polymerization of the top TFC layer.

The mean flow pore size of the support layer was determined to be 1.562 μm . In addition, the bubble point flow

rate was 0.019 L m^{-1} . The pore size distribution and porometry data are reflected in Fig. 9 and Table 2, respectively.

Pure water flux, water contact angles, porosity, mean fiber diameter, membrane substrate thickness, as well as other basic spinning solution properties are listed in Table 2. The substrate had high porosity of 67%, which yields a very high pure water permeability of 8.820 LMH bar^{-1} . Normally, sulfonation process increases the membrane hydrophilicity which is indicated by decrease of substrate contact angle, but this phenomenon is more pronounced in the support layer fabricated by phase inversion rather than electrospinning. The new developed sPSU membrane substrate has a contact angle of 119.07 ± 1.37 , which is lower than the contact angle given by membrane fabricated from non-sulfonated PSf (135.44 ± 0.11). The zeta potential of the membrane was determined at different values of pH. Negative zeta potential values of the substrate, which account for less than -50 mV at normal seawater pH 7.5–8.4, indicated that the membrane may have limited fouling propensity (Fig. 10).

Success of the PSf polymer sulfonation can be verified using FTIR. sPSU has peaks at 692, 1,014, 1,104, 1,149, 1,236, 1,487, and 2,968 cm^{-1} , which correspond to C–S, SO_3 , C–O, R– SO_2 –R, C–O, C–C (aromatic), and C–H (aliphatic), respectively. The presence of O=S=O stretching vibration

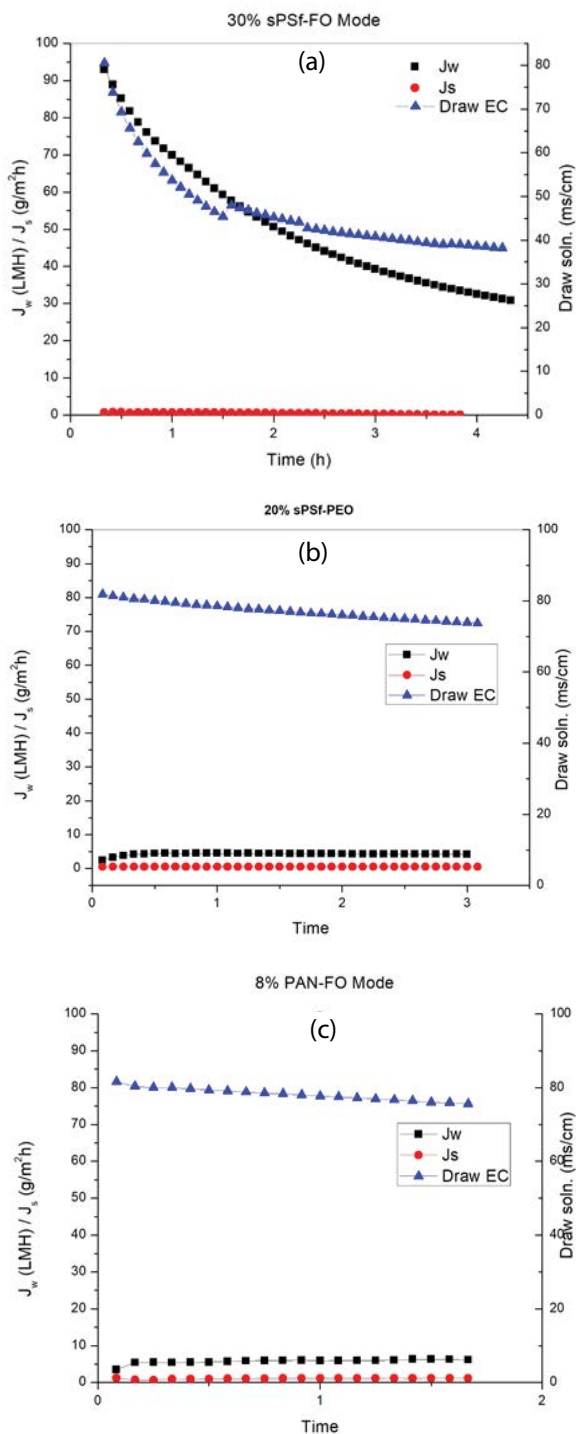


Fig. 7. J_w , J_s and DS concentration against time for (a) 30% sPSU, (b) 20% sPSU + PEO, and (c) 8% PAN, respectively.

of SO_3 groups near $1,014\text{ cm}^{-1}$ confirms the sulfonation of sPSU (Fig. 11). The SO_2 symmetric stretching was detected at $1,149.6\text{ cm}^{-1}$, which is corresponding to $1,150\text{ cm}^{-1}$ obtained by Naim et al. [28] and Eric et al. [29]. The infrared assignments of PSf and its sulfonated derivatives were illustrated in Table 3.

Combination of FTIR and SEM measurements was usually used to observe the interfacial polymerization of the polyamide thin film on the top of the sPSU substrate. Fig. 12 shows the ATR-FTIR spectra of the composite membrane which represent the thin polyamide layer and its support sPSU web. Peaks of the functional groups that represented the pure sPSU in Fig. 11 appeared in the spectrum of PA-sPSU with a minute shift. The new peaks at $1,660\text{ cm}^{-1}$ (C=O of amide), $1,609.9\text{ cm}^{-1}$ (aromatic ring breathing), and $1,542\text{ cm}^{-1}$ (C–N stretch of amide I) characterize the polyamide functional groups, which is in agreement with 1,161, 1,610, and $1,544\text{ cm}^{-1}$ measured by Naim et al. [28] and Eric et al. [29]. Table 4 presents main FTIR-observed spectrum distinguished to ultrathin polyamide in PA-sPSU membrane.

4.1.3. Characteristics of FO membranes

The surface morphology of the sPSU electrospun nanofiber-based TFC membranes was observed from SEM micrographs in Fig. 13. The membrane polyamide TFC layer has no pin hole. Forming a defect-free ridge and valley structure indicated that polyamide was successfully interfacially polymerized. The average measured thickness of the selective polyamide layer was 931.8 nm . High thickness of PA top film may be referred to a narrow range of substrate pore size distributions which is measured to be $1.167\text{--}2.092\text{ }\mu\text{m}$ with $1.562\text{ }\mu\text{m}$ as a mean pore size. Singh et al. [33] found that smaller pore size distributions of substrate have better salt separation efficiency compared with the wider pore size distribution, owing to a notable increase in TFC layer thickness following a reduced penetration of PA into pores of substrate.

Bui & McCutcheon [34] referred the increase in thickness of the polyamide surface set on the nanofiber support layer to the enhancement of the nanofiber hydrophilicity, which allows much more surface diffusion of the MPD molecules to the interface with TMC. A more vigorous interaction between MPD and TMC can be generated with rougher TFC topography without defects and pinholes.

4.2. Performance of FO membranes

4.2.1. Performance comparisons between FO membranes fabricated in this work and the other studies

Performance evaluation in terms of water permeation and RSF using 1 M NaCl draw solution and deionized (DIO) water feed solution among the membrane synthesized in this study and others, selected as a best performance flat sheet, reported in the previous studies, was shown in Table 5.

Advantageous performance of the membrane developed in this study over the other membranes can be pronounced, given that the concentration of draw solution used in our experiments (1 M NaCl) accounts for half the draw solution concentration utilized in comparison with previous studies (2 M NaCl). Table 5 also showed that this work membrane can achieve a high (FO/PRO) water flux of $65.7/313\text{ L m}^{-2}\text{ h}^{-1}$. Water flux, RSF, and DS concentration of newly developed membrane over operating time using FO cocurrent mode is shown in Fig. 14. During 3 h operation, water flux dropped from 79 to 42 LMH, while the draw concentration decreased from 83.5 to 39.2 ms/cm². Water flux results show

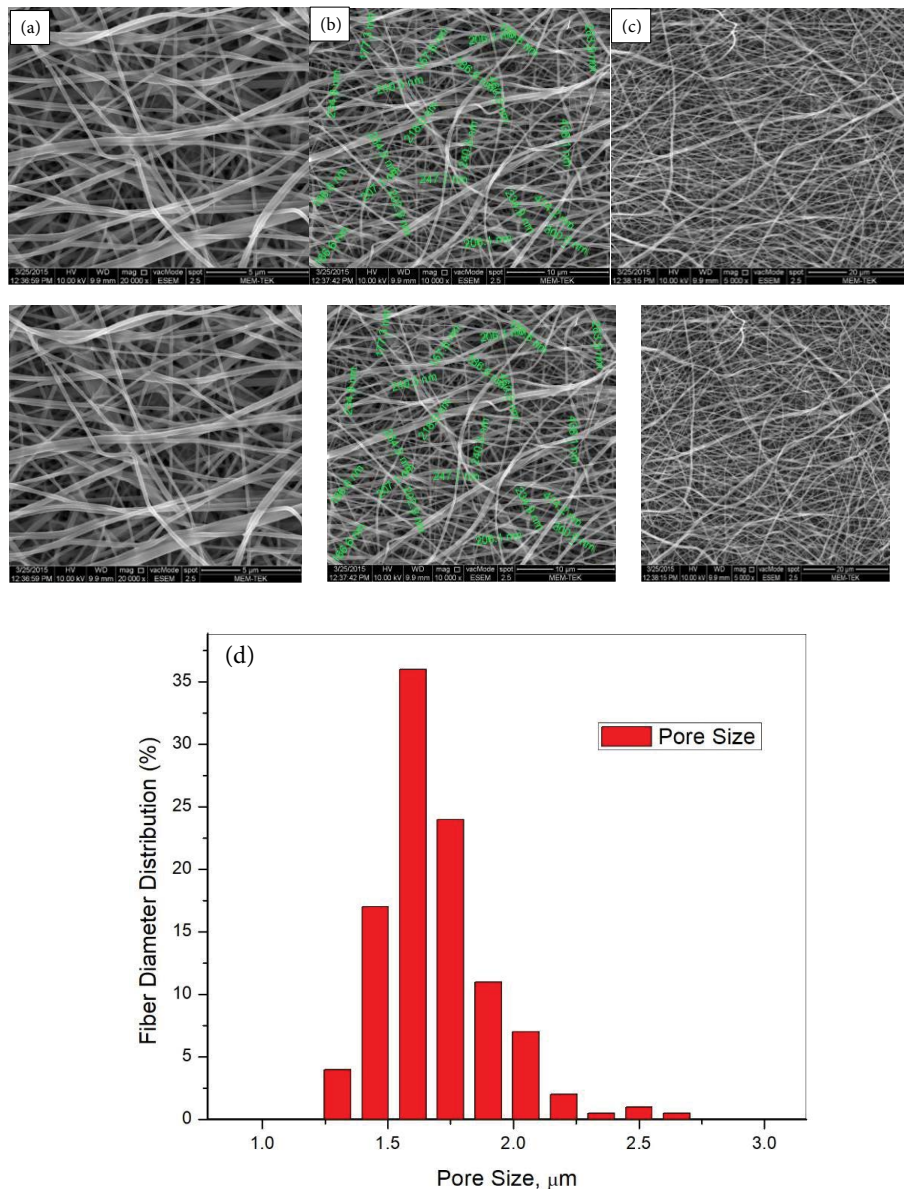


Fig. 8. (a) SEM micrographs of sPSU support membrane at (a) 20,000 \times , (b) 10,000 \times , (c) 5,000 \times magnification, and (d) histograms of the fiber diameter distributions.

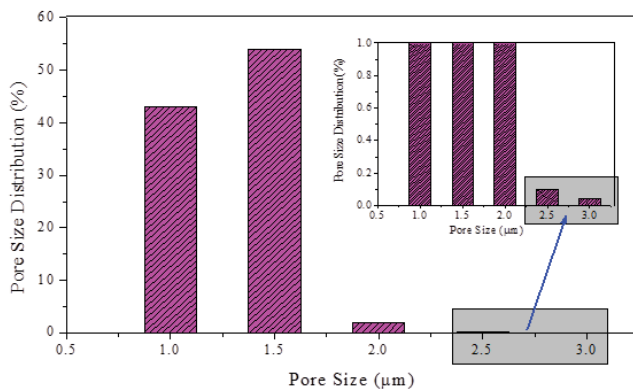


Fig. 9. Pore size distribution of the membrane support layer.

consistency with the decreasing of draw solution concentration. This revealed a good correlation in these membranes between water flux and DS concentration (osmotic pressure), which implies that the flux decline was not totally referred to ICP phenomenon, and it can be inferred that the membrane substrate enjoys a small structural parameter (S -value). Forward Osmosis Tech’s S -value calculator was used to estimate the new fabricated membrane S -value. The values of A , B , and J_w , aforementioned in the table above, were fed to online calculators, in addition to water temperature (298 k) and molarity of draw solution used during J_w determination (1 M).

Relatively low water flux value obtained in the FO mode, comparable with that value achieved in the PRO mode, may be referred to dilutive ICP within the boundary

Table 2
Summary of characterization tests of the spinning solution and sPSU membrane supports

Parameter	Value
<i>Spinning solution</i>	
Density	9.4 g cm ⁻³
Viscosity at 27.5°C	3,000 Cp
Conductivity	530 μs cm ⁻¹
Contact angle (°)	119.07 ± 1.37
Mean pore size (μm)	1.562
Maximum pore size (μm)	2.092
Minimum pore size (μm)	1.167
Pore density (number)	1.3E + 06
Flux (LMH)	8.820 LMH bar ⁻¹
Zeta potential	-26 @ pH 3 to -70 @ pH 10
Mean fiber diameter (nm)	247.4
Porosity (%)	66

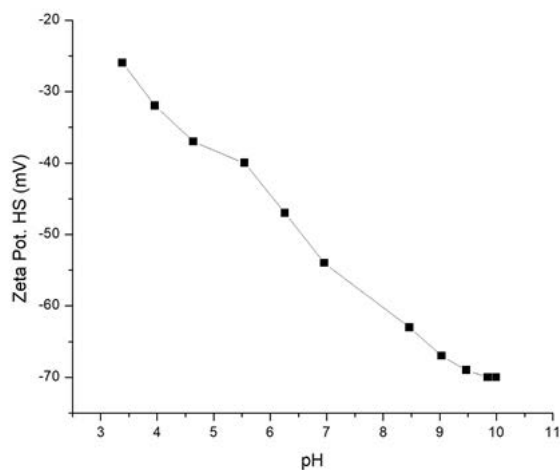


Fig. 10. Zeta potential measurement of sPSU support membrane.

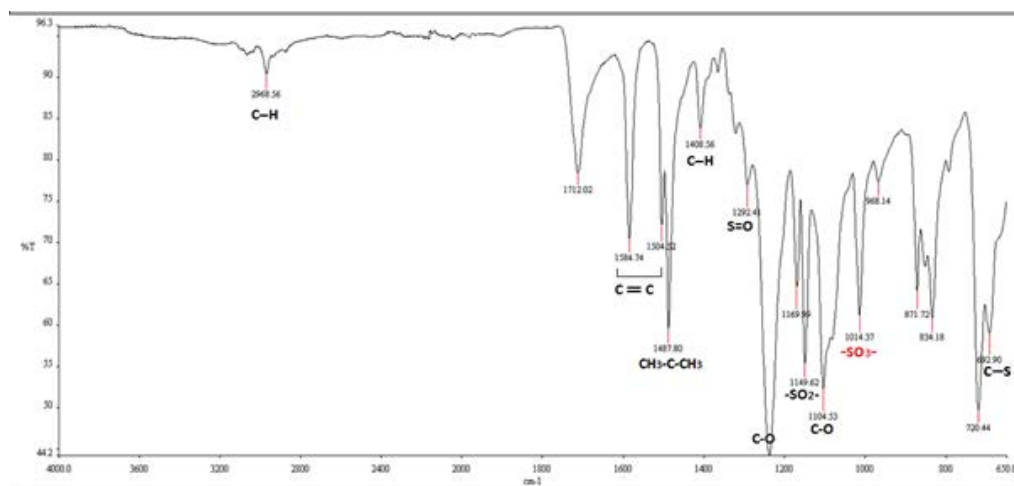


Fig. 11. FTIR spectra of the sPSU substrate membrane.

layer at the membrane surface which appears as a result of severe reduction of effective driving force when the AL-FS orientation experienced [35, 25].

Phillip et al. [36] considered the minimization of reverse solute flux from the draw solution into the feed solution in the osmotically driven membrane processes, a condition for effective operation of these systems.

The corresponding salt flux is only 2.5/5.3 gMH. Huang et al. [37] studied the impact of support layer pore size on TFC FO membranes. TFC FO membranes have higher rejection rate and lower reverse salt flux. Dilution effect happens while obtaining high water flux from the feed side, dilutes and hinders the salt which crossing the membrane, which enhances the salt rejection rate. As well, the high TFC layer thickness would be another reason that justifies high rejection and the low RSF performance of this membrane.

The new developed membrane demonstrated very high water flux, particularly in the PRO mode, which accounts for more than two-fold higher than the best previously fabricated membrane. Conjugated with a high rejection ratio (99.54%), it is noteworthy that the RSF obtained by our membrane is absolutely the lowest. This can be evident from the reverse flux selectivity represented by the ratio of water flux to RSF (J_w/J_s), which almost only rely on the intrinsic membrane active layer characteristics, *A* and *B*. Equivalent to 1 g NaCl pass to the feed, 26.3 and 58.8 L water will permeate to the draw in FO and PRO modes consequently. Even though the membranes fabricated in [14], [22], and [38] have a relatively high water flux, they still are far away from the result obtained by our fabricated membrane in terms of reverse flux selectivity (J_w/J_s).

Taking advantage of this merit, there is a potential to reduce the operational cost related to salts and chemicals used in draw solution preparation. Furthermore, concerns regarding using risky draw solution material such as ammonia could be alleviated.

In addition, with this high-throughput water flux, this membrane is greatly promising for application in the field of seawater desalination and energy production using PRO.

Table 3
Infrared assignments of polysulfone and its sulfonated derivative [28,30]

Frequency (cm ⁻¹)	Assignment
3,600–3,200	O–H stretching vibrations
2,980–2,880	Asymmetric and symmetric C–H stretching vibrations involving entire methyl group
1,590–1,485	Aromatic C=C stretching
1,412	Asymmetric C–H bending deformation of methyl group
1,365	Symmetric C–H bending deformation of methyl group
1,325–1,298	Double resulting from asymmetric O=S=O stretching of sulfone group
1,244	Asymmetric C–O–C stretching of aryl ether group
1,106	C–O stretching of aryl ether group*
1,170	Asymmetric O=S=O stretching of sulfone group
1,150	Symmetric O=S=O stretching of sulfone group
1,107–1,092	Aromatic ring vibration
1,027	Symmetric O=S=O stretching of sulfone group

*[27]

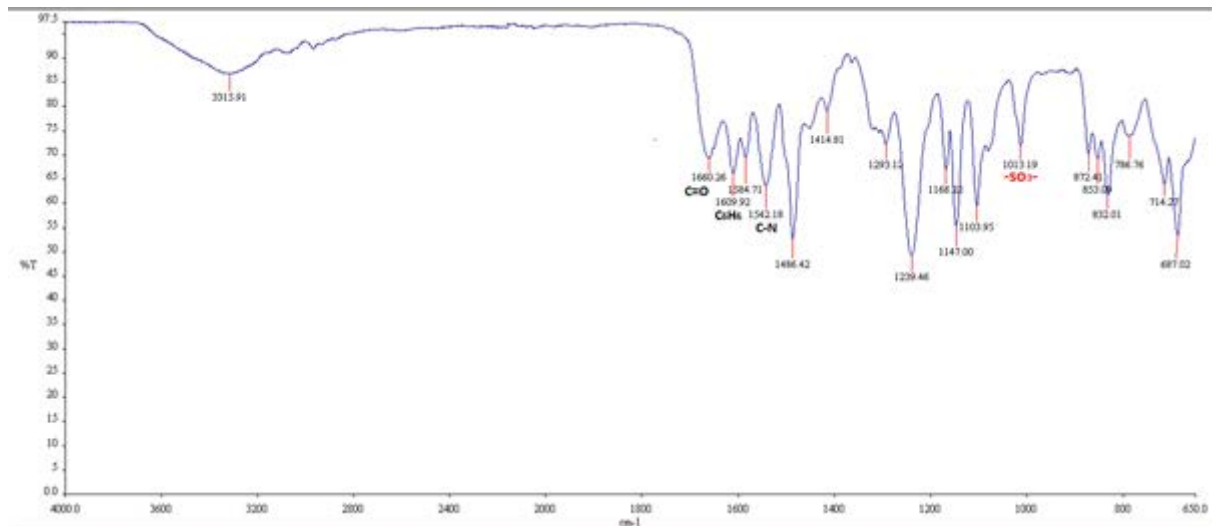


Fig. 12. FTIR spectra of the PA-sPSU composite membrane.

Table 4
Main FTIR-observed spectrum distinguished to ultrathin polyamide in PA-sPSU membrane [31,32]

Peak (cm ⁻¹)	Characteristics	This work PA-sPSU
1,535–1,555*	C–N axial deformation and CO–N–H angular deformation (amide II)	1,542.18
1,590–1,615**	Aromatic ring bending	1,609.92
1,630–1,680**	C=O stretching (amide I)	1,660.26

*[30], **[31].

The intrinsic membrane transport parameters, *A* and *B*, are shown in Table 6. Membranes with the highest *A* and the lowest *B* and *S*-values revealed the best FO performance. Our membranes have the highest *A* value of 4.97 LMHbar⁻¹ which is desirable for FO membranes to achieve high water

flux performance. Relation between intrinsic membrane transport parameters, *A* and *B* coefficients, among developed membranes and other membranes selected as the best performers in the literature was illustrated in Fig. 15. While some membranes showed a good *A* value with modest *B* value and vice versa, the membrane in this work showed a good desirable balance between *A* and *B*.

4.2.2. Performance of commercial FO membranes

Two commercial FO membrane kits (TFC-ES 130927 and CTA-ES 140127) were ordered from HTI. According to technical data sheet and operating instructions of these membranes, at a test condition of 1 M NaCl as draw solute and DI water as feed solution at 25°C, membrane area of 0.02 m² and CFV of 30 cm s⁻¹, the typical HTI CTA-ES membrane performance would achieve water flux of 9/12 and 18/36 LMH with 99% salt rejection when FO and PRO modes were applied, respectively, while water flux of 18/36

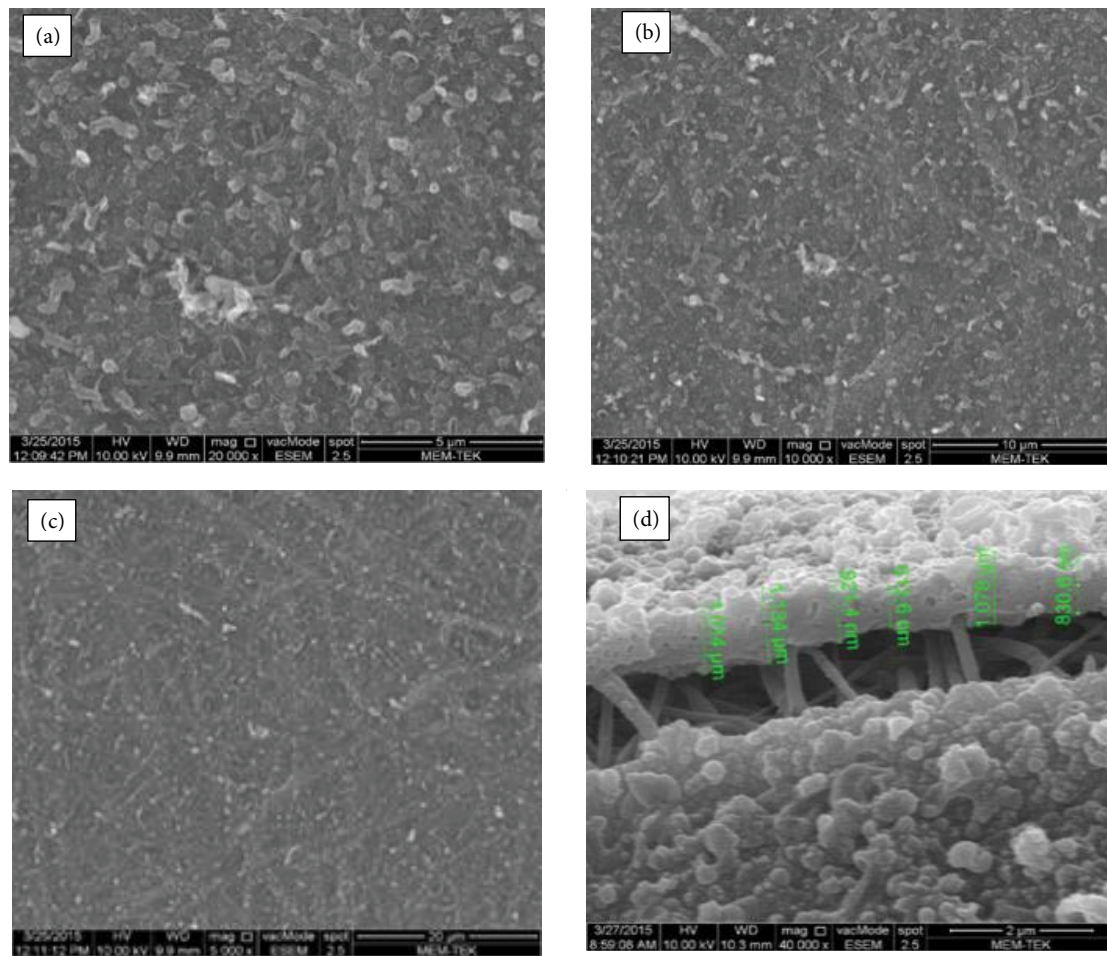


Fig. 13. Surface architecture (SEM micrographs) of TFC-FO membrane at (a) 20,000 \times , (b) 10,000 \times , (c) 5,000 \times magnification and cross-sectional SEM image of TFC electrospun porous support, (d) at magnifications of 40,000 \times .

Table 5
Comparisons of FO performance of various TFC-FO membranes with DI water as feed solutions

Membrane	Water flux, J_w (FO/PRO) (LMH)	Reverse salt flux, J_s (FO/PRO) (gMH)	J_s/J_w (g L ⁻¹)	J_w/J_s (L g ⁻¹)	Draw solution	References
FO flat-sheet membrane on sPSU	65.7/313	2.5/5.3	0.038/0.017	26.3/58.8	1.0 M NaCl	This work
CTA-ES HTI	10.27/8.10	7.11/20.03	0.69/2.47	1.44/0.4	1.0 M NaCl	CTA-ES HTI data sheet
TFC-ES HTI	7.22/19.31	8.39/14.78	0.125/0.765	0.86/1.3	1.0 M NaCl	TFC-ES HTI data sheet
FO flat-sheet membrane on cellulose ester substrate	80.1/128.8	10.0/19.4	0.125/0.15	8/6.67	2.0 M NaCl	[38]
FO flat-sheet membrane on sulfonated polyphenylsulfone (2.5 mole% direct sulfonation) supports	48/54	7.6/8.8	0.158/0.163	6.33/6.13	2.0 M NaCl	[22]
FO flat-sheet membrane on PES/sPSU supports	26.0/47.5	8.3/12.4	0.319/0.261	3.13/3.83	2.0 M NaCl	[14]

LMH and 99.4% salt separation could be realized by HTI TFC-ES at the same conditions. Performance of these two membranes was explored for 3 h under aforementioned experimental conditions of the current study without further manipulation and cleaning when it alternates from FO mode to PRO mode. As shown in Table 7, HTI CTA-ES membrane obtained flux of 10.54 LMH in FO mode and 11.58 LMH in PRO mode, close to the values mentioned in the data sheet. Operation of HTI CTA-ES membrane in the FO mode for 3 h gave average RSF of 0.42 gMH and J_s/J_w of 0.04 g L⁻¹. Shifting directly for PRO operation without inter-back flushing or chemical cleaning was the cause of profound concentration polarization effect that raised the average RSF of 4.98 gMH and restricted water flux to 11.58 LMH in PRO mode (Fig. 16). Impact of concentration polarization was manifested early in TFC-ES membrane as it achieved average reverse

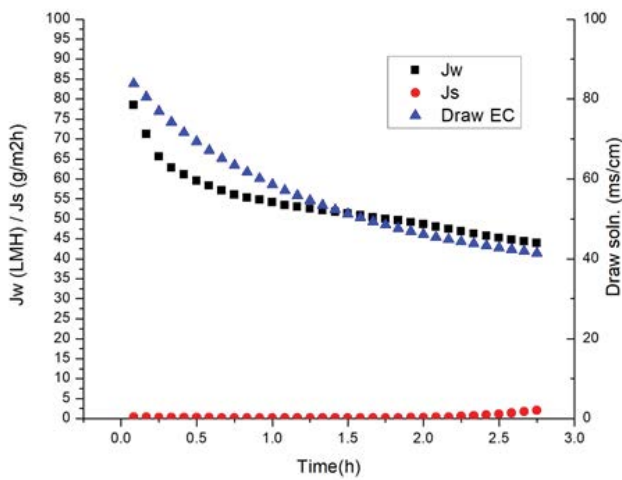


Fig. 14. Developed TFC-FO membrane water flux, RSF, and DS concentration over operating time using FO cocurrent mode.

Table 6

The transport parameters *A* and *B* and salt rejection percent of newly developed sPSU nanofiber-based FO-TFC membranes measured from cocurrent FO mode

Membrane	Water permeability, <i>A</i> ^a (L m ⁻² h ⁻¹ bar ⁻¹)	Salt permeability, <i>B</i> ^b (L m ⁻² h ⁻¹)	(<i>A</i> / <i>B</i>) ^{FO} (bar ⁻¹)	Rejection (%)	References
FO flat-sheet membrane on sPSU	4.97	0.287	17.31	99.54 ^b	This work
FO flat-sheet membrane on cellulose ester substrate	2.85	0.345	8.26	–	[38]
FO flat-sheet membrane on sulfonated polyphenylsulfone (2.5 mole% direct sulfonation) supports	3.23	1.05	3.07	84.1 ^c	[22]
FO flat-sheet membrane on PES/sPSU supports	0.77	0.11	7	93.5 ^d	[14]
CTA	0.97 ^e	1.16 ^f	0.836		[4]

^aTested by a dead-end permeation cell (Sterlitech stirred cell) at three different pressure points using DI water.

^bCalculated based on experiments under the FO mode using 1 M NaCl as the draw solution and DI water as the feed.

^cTested at 25 psi (1.72 bar) with 400 ppm NaCl solution.

^d1,000 ppm salt as the feed solution in the RO test at 5 bar.

^eDone by Journal of Membrane Science 444 (2013) 523–538.

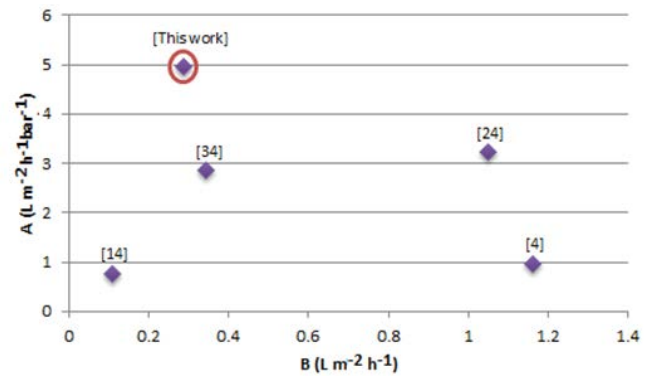


Fig. 15. The relation between the intrinsic membrane transport parameters; *A* and *B* coefficients of the membrane in this study and other selected high-performance membranes in the literature.

salt flux of 13.30 gMH in the FO mode and exacerbated to reach 31.09 gMH in PRO. The modest performance of TFC-ES was also revealed through very high J_s/J_w of 0.9814 and 1.2789 in both FO and PRO modes, respectively. Even though it reveals higher water flux proportional to CTA-ES membrane, buildup of salt concentration was more rapid in TFC-ES membrane, which would be in need for more frequent cleaning cycles.

This effect was more visible in HTI TFC-ES whose performance was far away from data sheet figures. In both the membranes, RSF was higher during PRO testing compared with FO, mainly due to ICP effects.

Philip et al. [36] tested the flat-sheet commercial HTI CTA membrane performance in the FO mode using 2 M NaCl as a draw solution. The membrane has a pure water flux of 13 LMH and RSF of 10.5 gMH.

Performance comparison among different osmotically driven membranes is a matter of complexity due to its broad

Table 7
FO performance characterization results of commercial HTI CTA-FO membrane

Mode	J_w (LMH)	J_s (gMH)	J_s/J_w (g L ⁻¹)	SR %	B	Time
HTI CTA-FO mode	10.54	0.427	0.04	99.89	0.0102	3 h
HTI CTA-PRO	11.58	4.98	0.4303	98.89	0.1287	2.8 h
HTI TFC-FO mode	13.55	13.30	0.9814	98.29	0.2333	2.6 h
HTI TFC-PRO mode	24.30	31.09	1.2789	95.51	1.1346	2.5 h

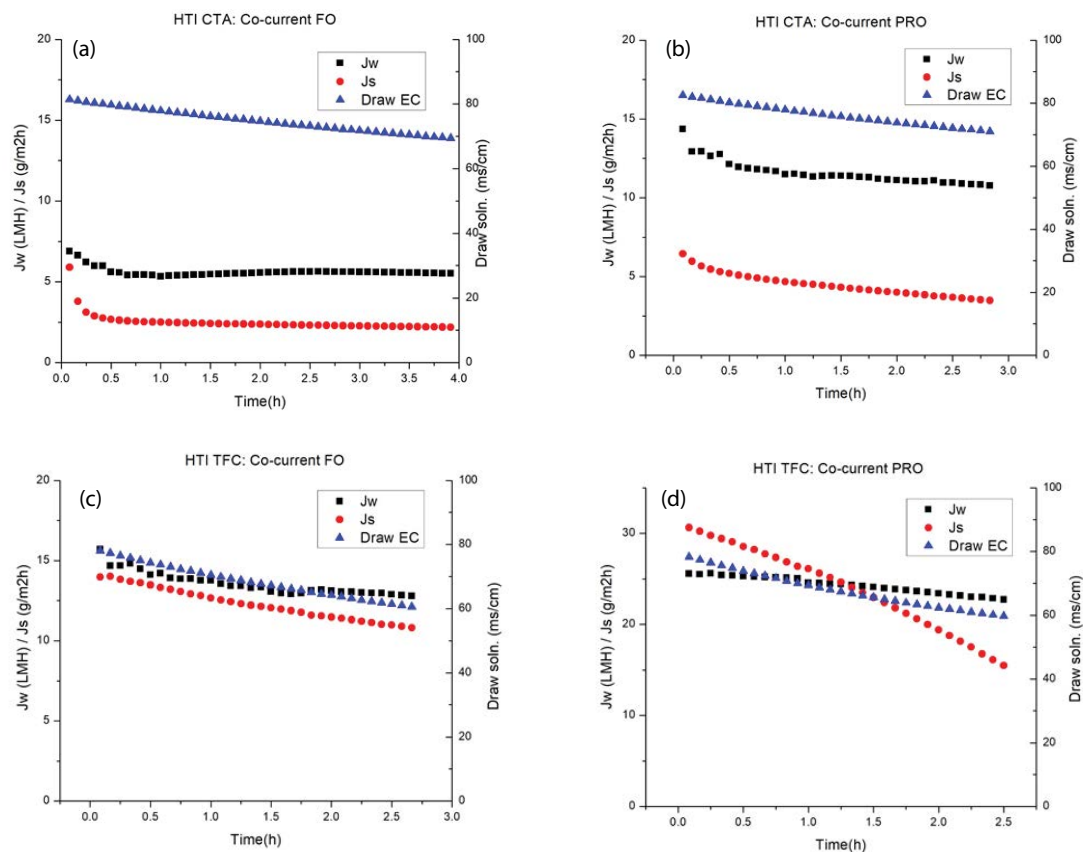


Fig. 16. Water flux, salt flux, and DS concentration against operating time of commercial HTI CTA/TFC membranes. (a) HTI CTA in cocurrent FO mode, (b) HTI CTA in cocurrent PRO mode, (c) HTI TFC in cocurrent FO mode, and (d) HTI TFC in cocurrent PRO mode.

membrane properties and wide range of applicable operating conditions. Cath et al. [39] made an attempt to introduce standard method for evaluating membrane performance in osmotically driven membrane processes. They concluded that performance data of asymmetric CSA membrane under different operation conditions are less scattered in comparison to those from the TFC membranes, particularly in terms of water flux.

5. Conclusions

By implementation of new material and structure, proper fabrication of membrane substrate can play a crucial role in the development of TFC-FO membranes. Current work has revealed that hydrophilic sPSU is a reliable substrate material for the synthesis of high-performance TFC-FO membranes.

The following conclusions can further be drawn from this work:

- In the scaffold nanofiber-based TFC-FO membrane, control of fiber diameter thickness at ≤ 300 nm and having pore size at the narrow distribution range could generate good formation of a TFC layer on the top of the substrate.
- The current study membrane demonstrated high water permeance and salt separation. It is compared favorably with commercial membranes and the membranes mentioned in the literature. Under aforementioned FO setup test conditions, the membrane obtained water flux of 65.7 and 313 LMH with low RSF of 2.5 and 5.3 gMH using 1 M sodium chloride against DW in AL-FS and AL-DS operation modes, respectively.

- Performance assessment among the different membranes must be made on a comparable basis. Different studies tested the membrane desalination performance under very versatile test conditions (it includes, but not restricted to, the test period, draw solution concentration and type, CFV, membrane surface, membrane orientation, and circulation mode). For easy comparison between different membrane performances, standardization of evaluation method could be done by defining a membrane performance protocol.
- To take this high-performance membrane to the next stage of real-world desalination application, further research is needed to develop cleaning and fouling protocol.
- With its high water flux, particularly in PRO mode, the applicability of this new membrane could be established for PRO with more limited applied pressure, in purpose of energy production, if more research efforts could be exerted to elevate its mechanical strengths using nanocomposites.

Acknowledgment

The authors are grateful to TUBITAK (The Scientific and Technological Research Council of Turkey) for their financial support under grant (Project No: 113Y356).

Symbols

A	—	Water permeability, $\text{m s}^{-1} \text{atm}^{-1}$
B	—	Solute permeability, m s^{-1}
J_w	—	Water flux, $\text{Lm}^{-2}\text{h}^{-1}$, LMH^{-1}
J_s	—	Reverse salt flux, $\text{gm}^{-2}\text{h}^{-1}$, gMH^{-1}
K	—	Solute resistivity, s m^{-1}
L	—	Channel length, m
Re	—	Reynolds number
S	—	Membrane structure parameter, m
Cp	—	Centipoise
LMH	—	Liters per square meter hour
gMH	—	Grams per square meter hour
J_w/J_s	—	Reverse flux selectivity

Greek

ε	—	Porosity
η	—	Viscosity, Pa s
π	—	Osmotic pressure, bar
ρ	—	Density, kg m^{-3}
τ	—	Tortuosity

Subscripts

FO	—	Forward osmosis mode
PRO	—	Pressure-retarded osmosis mode
FS	—	Feed solution
DS	—	Draw solution
ICP	—	Internal concentration polarization
ECP	—	External concentration polarization
CFV	—	Cross-flow velocity
SR	—	Salt rejection
TFC	—	Thin-film composite
RO	—	Reverse osmosis

sPSU	—	Sulfonated polysulfone
PAN	—	Polyacrylonitrile
PEO	—	Poly(ethylene oxide)
ENM _s	—	Electrospun nanofiber membranes

References

- [1] J. Duan, E. Litwiller, I. Pinnau, Preparation and water desalination properties of POSS-polyamide nanocomposite reverse osmosis membranes, *J. Membr. Sci.*, 473 (2015) 157–164.
- [2] R.V. Linares, Z. Li, S. Sarp, S.S. Bucs, G. Amy, J.S. Vrouwenvelder, Forward osmosis niches in seawater desalination and wastewater reuse, *Water Res.*, 66 (2014) 122–139.
- [3] S. Zhao, L. Zou, D. Mulcahy, Brackish water desalination by a hybrid forward osmosis–nanofiltration system using divalent draw solute, *Desalination*, 284 (2012) 175–181.
- [4] M. Chérif, I. Mkacher, L. Dammak, A.B. Salah, K. Walha, D. Grande, V. Nikonenko, Water desalination by neutralization dialysis with ion-exchange membranes: flow rate and acid/alkali concentration effects, *Desalination*, 361 (2015) 13–24.
- [5] M. Sadrzadeh, T. Mohammadi, Sea water desalination using electro-dialysis, *Desalination*, 221 (2008) 440–447.
- [6] K.S. Maheswari, K.K. Murugavel, Thermal desalination using diesel engine exhaust waste heat — An experimental analysis, *Desalination*, 358 (2015) 94–100.
- [7] Y. Tokui, H. Moriguchi, Y. Nishi, Comprehensive environmental assessment of seawater desalination plants: Multistage flash distillation and reverse osmosis membrane types in Saudi Arabia, *Desalination*, 351 (2014) 145–150.
- [8] M. Tian, C. Qiu, Y. Liao, S. Chou, R. Wang, Preparation of polyamide thin film composite forward osmosis membranes using electrospun polyvinylidene fluoride (PVDF) nanofibers as substrates, *Sep. Purif. Technol.*, 118 (2013) 727–736.
- [9] X.R. Zhang, L.Z. Zhang, H.-M. Liu, L.-X. Pei, One-step fabrication and analysis of an asymmetric cellulose acetate membrane for heat and moisture recovery, *J. Membr. Sci.*, 366 (2011) 158–165.
- [10] E. Woode, Forward osmosis (FO) membrane designs and materials, <http://www.forwardosmosistech.com/forward-osmosis-fo-membrane-designs-and-materials> (Accessed in 2014).
- [11] I.V. Farr, U.J. Bharwada, T. Gullinkala, Method to Improve Forward Osmosis Membrane Performance, U.S. Patent: 13/559,472, 26 7 2012.
- [12] W.J. Lau, A.F. Ismail, N. Misdan, M. Kassim, A recent progress in thin film composite membrane: a review, *Desalination*, 287 (2012) 190–199.
- [13] B.J.A. Tarbousha, D. Ranaa, T. Matsuura, H.A. Arafat, R.M. Narbaitz, A polyfunctional amine and a polyfunctional acid chloride, dissolved in water and hydrocarbon solvent, respectively (Preparation of thin-film-composite polyamide membranes for desalination using novel hydrophilic surface modifying macromolecules), *J. Membr. Sci.*, 325 (2008) 166–175.
- [14] K.Y. Wang, T.S. Chung, G. Amy, Developing thin-film-composite forward osmosis membranes on the PES/SPSf substrate through interfacial polymerization, *AIChE J.*, 58 (2012) 770–781.
- [15] Z.X. Low, Q. Liu, E. Shmsaei, X. Zhang, H. Wang, Preparation and characterization of thin-film composite membrane with nanowire-modified support for forward osmosis process, *Membranes*, 5 (2015) 136–149.
- [16] J.R. McCutcheon, M. Elimelech, Influence of membrane support layer hydrophobicity on water flux in osmotically driven membrane processes, *J. Membr. Sci.*, 318 (2008) 458–466.
- [17] S. Kaur, M. Zuwei, R. Gopal, G. Singh, S. Ramakrishna, T. Matsuura, Plasma-induced graft copolymerization of poly(methacrylic acid) on electrospun poly(vinylidene fluoride) nanofiber membrane, *Langmuir*, 23 (2007) 13085–13092.
- [18] S. Subramanian, R. Seeram, New directions in nanofiltration applications — Are nanofibers the right materials as membranes in desalination, *Desalination*, 308 (2013) 198–208.

- [19] M. Hasani-Sadrabadi, I. Shabani, M. Soleimanid, H. Moaddel, Novel nanofiber-based triple-layer proton exchange membranes for fuel cell applications, *J. Power Sources*, 196 (2011) 4599–4603.
- [20] M.H. Chen, T.C. Chiao, T.W. Tseng, Preparation of sulfonated polysulfone/polysulfone and aminated polysulfone/polysulfone blend membranes, *J. Appl. Polym. Sci.*, 61 (1996) 1205–1209.
- [21] N. Widjojoa, T. Chunga, M. Weberb, C. Maletzko, V. Warzelhanb, The role of sulphonated polymer and macrovoid-free structure in the support layer for thin-film composite (TFC) forward osmosis (FO) membranes, *J. Membr. Sci.*, 383 (2011) 214–223.
- [22] N. Widjojoa, T. Chunga, M. Weberb, C. Maletzko, V. Warzelhanb, A sulfonated polyphenylenesulfone (sPPSU) as the supporting substrate in thin film composite (TFC) membranes with enhanced performance for forward osmosis (FO), *Chem. Eng.*, 220 (2013) 15–23.
- [23] G. Han, T. Chung, M. Toriida, S. Tamai, Thin-film composite forward osmosis membranes with novel hydrophilic supports for desalination, *J. Membr. Sci.*, 423 (2012) 543–555.
- [24] Y.C. Kim, S.J. Park, Experimental study of a 4040 spiral-wound forward-osmosis membrane module, *Environ. Sci. Technol.*, 45 (2011) 7737–7745.
- [25] R. Wang, L. Shi, C.Y. Tang, S. Chou, C. Qiu, A.G. Fane, Characterization of novel forward osmosis hollow fiber membranes, *J. Membr. Sci.*, 355 (2010) 158–167.
- [26] A.K. Ghosh, R.C. Bindal, S. Prabhakar, P.K. Tewari, Composite polyamide reverse osmosis (RO) membranes – recent developments and future directions, *BARC Newsletter*, 321 (2011) 43–51.
- [27] I. Shabani, M.M. Hasani-Sadrabadi, V. Haddadi-Asl, M. Soleimani, Nanofiber based polyelectrolytes as novel membranes for fuel cell applications, *J. Membr. Sci.*, 368 (2011) 233–240.
- [28] R. Naim, A.F. Ismail, H. Saidi, E. Saion, (Development of sulfonated polysulfone membranes as a material for proton exchange membrane (PEM), Proceedings of the Regional Symposium on Membrane Science Technology, Puteri Pan Pacific Hotel, JohorBharu, Malaysia, 2004)
- [29] H. Eric, B. Ngoc, J.R. McCutcheon, M.L. Lind, Nanostructured Membranes for Engineered Osmosis Applications, Patent: 13/508,892, 2010.
- [30] D. Fikai, A. Fikai, G. Voicu, B.S. Vasile, C. Guran, E. Andronescu, Polysulfone based membranes with desired pores characteristics, *Mater. Plast.*, 47 (2010) 24–27.
- [31] L.M. Guerrini, M.C. Branciforti, T. Canova, R.E. Bretas, Electrospinning and characterization of polyamide 66 nanofibers with different molecular weights, *Mater. Res.*, 12 (2009) 181–190.
- [32] J.B. Lambert, Introduction to organic spectroscopy, Macmillan, New York, 1987.
- [33] Singh, P.S. Joshi, S.V. Trivedi, J.J. Devmur, Probing the structural variations of thin film composite RO membranes obtained by coating polyamide over polysulfone membranes of different pore dimensions, *J. Membr. Sci.*, 278 (2006) 19–25.
- [34] N.N. Bui, J. McCutcheon, Hydrophilic nanofibers as new supports for thin film composite membranes for engineered osmosis, *Environ. Sci. Technol.*, 47 (2013) 1761–1769.
- [35] S. Chou, L. Shi, R. Wang, C.Y. Tang, C. Qiu, A.G. Fane, Characteristics and potential applications of a novel forward osmosis hollow fiber membrane, *Desalination*, 261 (2010) 365–372.
- [36] W.A. Phillip, J.S. Yong, M. Elimelech, Reverse draw solute permeation in forward osmosis: modeling and experiments, *Environ. Sci. Technol.*, 44 (2010) 5170–5176.
- [37] L. Huang, N.N. Bui, M.T. Meyering, T.J. Hamlin, J.R. McCutcheon, Novel hydrophilic nylon 6, 6 microfiltration membrane supported thin film composite membranes for engineered osmosis, *J. Membr. Sci.*, 437 (2013) 141–149.
- [38] R.C. Ong, T.S. Tai-Shung Chung, J.S. Wit, B.J. Helmer, Novel cellulose ester substrates for high performance flat-sheet thin-film composite (TFC) forward osmosis (FO) membranes, *J. Membr. Sci.*, 473 (2015) 63–71.
- [39] T.Y. Cath, M. Elimelech, J.R. McCutcheon, R.L. McGinnis, A. Achilli, D. Anastasio, J. Lampi, Standard methodology for evaluating membrane performance in osmotically driven membrane processes, *Desalination*, 312 (2013) 31–38